Applied Catalysis B: Environmental 84 (2008) 616–630

Contents lists available at ScienceDirect

Applied Catalysis B: Environmental

journal homepage: www.elsevier.com/locate/apcatb

NO_x storage and reduction with H_2 on $Pt/BaO/Al_2O_3$ monolith: Spatio-temporal resolution of product distribution☆

Robert D. Clayton, Michael P. Harold *, Vemuri Balakotaiah *

Department of Chemical & Biomolecular Engineering, University of Houston, Houston, TX 77204-4004, United States

ARTICLE INFO

Article history:
Received 9 January 2008
Received in revised form 3 May 2008
Accepted 19 May 2008
Available online 28 May 2008

Keywords:
NO_x
Hydrogen
Platinum
Barium
Selective catalytic reduction
NO_x storage and reduction
Lean NO_x trap

ABSTRACT

The regeneration of a model $Pt/BaO/Al_2O_3$ monolith catalyst was studied with hydrogen as the reductant to elucidate the reaction pathways to molecular nitrogen and ammonia. NO_x storage and reduction experiments (NSR) were conducted with a 2 cm length monolith for a wide range of feed conditions. The NSR experiments were replicated for a series of monoliths of progressively decreasing length, enabling the construction of spatio-temporal profiles of reactant and product concentrations. The results show that there are two primary competing routes to the desired N_2 product; specifically a direct route from the reduction of stored NO_x by H_2 ($H_2 + NO_x \rightarrow N_2$) or by a sequential route through NH_3 ($H_2 + NO_x \rightarrow NH_3$; $NH_3 + NO_x \rightarrow N_2$). A comparison between H_2 and NH_3 as reductant feeds during NSR revealed H_2 is a more effective reductant in terms of NO_x conversion for temperatures below approximately 230 °C. At higher temperatures (230–380 °C), the regeneration of stored NO_x is feed-limited and the difference between the reductants H_2 and NH_3 is found to be small with H_2 being a slightly superior reductant. Experimental measurements of the traveling front velocity are compared with a simple feed-limited model that assumes complete consumption of H_2 as stored NO_x is depleted. At lower temperatures the regeneration is limited by chemical processes at the Pt/Ba interface. The findings are pieced together to establish a phenomenological description of the spatio-temporal features of the lean NO_x trap with hydrogen as the reductant.

1. Introduction

Lean burn combustion encountered in lean burn gasoline and diesel vehicles provides for a higher fuel efficiency compared to stoichiometrically operated gasoline engines. However, the unconverted oxygen in the exhaust prevents the use of conventional three-way catalysts (TWC) in the reduction of NO_x to N_2. NO_x storage and reduction (NSR) is a periodic catalytic process for converting NO and NO_2 (NO_x) to N_2 that overcomes this obstacle. The inherent transient nature of NSR makes it highly complex, especially in terms of the spatio-temporal interactions of the storage and reduction catalytic processes. Advanced catalytic engineering is needed to elucidate the transient product distribution in particular since in most cases the objective is to convert NO_x to molecular nitrogen.

During NSR, the NO_x removal process involves two stages on a bifunctional supported catalyst. The first "storage" stage involves the reactive trapping of NO_x, in the form of nitrites or nitrates, on an alkali earth component (such as Ba, Ca, or Sr) enhanced by the catalytic oxidation of NO to NO_2 on the precious metal (Pt, Rh). The typical duration of this stage is 30–90 s. The second "purge" or "regeneration" stage involves purging or regenerating with a rich pulse containing reductant(s), carried out before an unacceptable amount of NO_x breaks through during the storage. The rich pulse duration is only a few seconds. It is created through intermittent rich operation of the engine, producing a mixture of H_2, CO, and low molecular weight hydrocarbons, or through direct injection of fuel into the exhaust system.

Earlier studies of NSR focused on the storage process, which established that the primary steps are the catalytic oxidation of NO to NO_2 followed by NO_2 storage by the disproportionation

☆ *Disclaimer*: This report was prepared as an account of work sponsored by an agency of the United State Government. Neither the United States Government nor any agency thereof, nor any of their employees, makes any warranty, express or implied or assumes any legal liability or responsibility for the accuracy, completeness, or usefulness of any information, apparatus, product, or process disclosed, or represents that its use would not infringe privately owned rights. References herein to any specific commercial product, process, or service by trade name, trademark, manufacturer, or favoring by the United States Government or any agency thereof. The views and opinions of authors expressed herein do not necessarily state or reflect those of the United States Government or any agency thereof.

* Corresponding authors. Tel.: +1 7137434307; fax: +1 7137434323.
E-mail addresses: mharold@uh.edu (M.P. Harold), bala@uh.edu (V. Balakotaiah).

0926-3373/$ – see front matter © 2008 Elsevier B.V. All rights reserved.
doi:10.1016/j.apcatb.2008.05.018

mechanism [1–5]. The mechanistic details at the Pt/Ba interface remain elusive. Recent research has shifted to the kinetics of the regeneration process. Particular attention has been placed on H_2 because it is not only present in the exhaust during rich engine operation, but also it is catalytically generated by both steam reforming of exhaust hydrocarbons and water gas shifting of CO. Hydrogen has been shown to be the most effective reductant due to its high reactivity with O, H, and N adspecies which are present during conventional NSR operation. Hydrogen is uniquely reactive at low temperatures (below 200 °C) [6–9]. The mechanism of NO_x reduction under cycling conditions is still not fully understood. Muncrief et al. [10] suggested a thermally driven process under conditions in which a relatively large concentration of O_2 is present during the rich pulse, which is more typical of diesel applications. Liu and Anderon [7] proposed a spillover mechanism of reductant from the precious metal (Pt) to storage phase comprising barium nitrate, $Ba(NO_3)_2$. Their proposed mechanism involves the reductant reacting directly with $Ba(NO_3)_2$ forming $Ba(NO_2)_2$, which then releases the stored NO_x as NO. Nova et al. [11,12] studied the reduction process under nearly isothermal conditions and observed that the thermal decomposition of stored NO_x was not necessary to reduce the stored NO_x with H_2 since regeneration can occur at temperatures well below the temperature at which stored NO_x decomposes. They proposed that the reduction of stored nitrates involves a Pt catalyzed surface reaction and argued that the pathway only occurs when both components (Pt and BaO) are well dispersed on the same support (as opposed to physical mixtures of separate populations of supported Pt and BaO particles). A follow up study by Cant et al. [13] observed results similar to those of Nova et al. [11] when comparing a sample with Pt and BaO dispersed on the same support with a physical mixture of BaO/Al_2O_3 and Pt/SiO_2; Pt/SiO_2 was used instead of Pt/Al_2O_3 in order to rule out NO_x storage on the same support as Pt. The reverse spillover of NO_x from BaO to Pt has also been speculated to occur [13–17]. Cant et al. [13] studied the isotopic exchange rate of ^{15}NO and stored $^{14}NO_x$ during storage on the two system described above at 360 °C. They concluded that the forward and reverse spillover of NO_x is important since the exchange rate was more than five times faster for the $Pt/BaO/Al_2O_3$ sample than for the physical mixture. James et al. [14] proposed the "reverse" spillover mechanism to explain the decomposition of nitrates stored far from Pt. Zhou et al. [17] have described the nitrate ions as being mobile in the barium phase with the reaction occurring at the Pt/Ba interface. However, neither H_2 spillover to BaO nor the reverse spillover of NO_x to Pt has been proven to be the main mechanism. Medhekar et al. [18] studied pre-reduced, pre-oxidized, and pre-nitrated Pt/BaO catalysts, and proposed that there existed two distinct reduction sites on Pt crystallites on the supported catalyst. The first type of sites are located further from the Pt/Ba interface where H_2 scavenging of surface oxygen provides a clean surface for NO decomposition to N_2 and N hydrogenation to NH_3. The second type of sites is located at the Pt/BaO interface. At these sites H_2 oxidation, nitrate decomposition, and NO decomposition and reduction occur, producing a complex mixture of N_2, N_2O, and NH_3 which depends on the temperature and effective NO_x/H ratio.

The situation is further complicated by integral effects brought about by chemistry occurring downstream in the monolith channel, Choi et al. [19] applied spatially-resolved mass spectrometry, coined "Spaci-MS", to obtain spatial profiles of reactant and product profiles through the use of capillary probes positioned in multiple monolith channels along the length of the monolith. In their study, Choi et al. [19] showed that H_2 produced from the water gas shift reaction had only a minor effect on the NO_x release and reduction.

The effects of H_2O and CO_2 on the reduction of stored NO_x by H_2 have been investigated [20–22]. Lindolm et al. [20] observed that CO_2 had a promoting effect on NH_3 formation at low temperatures. Lietti et al. [21] observed that the reduction of stored NO_x is slower when CO_2 and H_2O are fed during the regeneration.

More recent studies have been carried out that have focused on the role of ammonia during NSR. Ammonia is an undesired product during conventional NO_x trap operation, however, it is a desired product in coupled LNT/SCR systems [23–25]. Pihl et al. [26] and Cumaranatunge et al. [27] proposed that NH_3 formed upstream by the reaction of feed H_2 and stored NO_x may be consumed downstream by its own reduction of stored NO_x [26,27]. Once formed, the generated N_2 flows down the reactor and out with the effluent. NH_3 has the complicating feature that it will readsorb and react downstream with stored NO_x. Pihl et al. [26] described the monolith reaction system by three sections: mostly regenerated, reductant front, and un-regenerated. They proposed that the reductant H_2 front moves through the entrance section of the monolith where the main reduction chemistry occurs. Cumaranatunge et al. [27] described the NH_3 as a hydrogen carrier, from which H adatoms react with stored NO_x to produce N_2. They showed that the effectiveness of NH_3 and H_2 under reductant limited conditions (350 °C) were similar. However, data were not presented by either of the two groups that conclusively prove the proposed picture. Xu et al. [28] showed that the steady-state selectivity of the reaction between H_2 and NO to N_2O, N_2, and NH_3 is largely dictated by the feed composition (H_2/NO ratio) and temperature under steady-state conditions. Clayton et al. [29] have shown that the reduction of NO by a co-feed of H_2 and NH_3 identifies H_2 as the superior reductant. To this end, under the complex spatio-temporal conditions encountered during the hydrogen regeneration of the NO_x trap, isolating the production of ammonia from its consumption is key to understanding the NO_x trap performance.

The objective of this study is to establish a more complete picture supported by experimental measurement of lean NO_x trap behavior during NSR using H_2 as a reductant. This is accomplished through bench-scale LNT measurements in which the concentrations of all reactants and products are measured. We utilize a novel approach to generate axial profiles of species concentrations over a range of conditions. An analysis of the product distribution reveals the different routes to the desired N_2 product, whether directly from the reduction of stored NO_x by H_2 or indirectly through an NH_3 intermediate. The data also provide information about the velocity of the moving hydrogen and ammonia fronts. The findings are pieced together to establish a phenomenological description of the spatio-temporal features of the lean NO_x trap with H_2 as the reductant.

2. Experimental

2.1. Catalyst samples

The catalyst samples used for these experiments were monolith catalysts provided by BASF Catalysts LLC (Iselin, New Jersey). Larger cylindrical cores (D = 3.8 cm, L = 7.6 cm) were cut using a dry diamond saw to smaller, nearly cylindrical shapes ($D \sim 0.8$ cm, L = 0.33–2 cm). The samples contained BaO with varying amounts of Pt on a γ-alumina washcoat support adsorbed on a cordierite structure (~62 channels/cm^2). The mass of washcoat material (m_{wc}) on each monolith piece (of L = 2 cm) was approximately 110 mg. The compositions and properties of the catalysts are given in Table 1. The methods used to characterize the catalysts were described previously [28]. The monoliths were then wrapped in Fiberfrax® ceramic paper that had been heat treated and then placed in a quartz tube flow reactor.

Table 1
Two catalyst used and their properties

Sample	Pt (wt.%)	BaO (wt.%)	Pt dispersion (%)	Pt area (m^2/g)	Pt particle size (nm)	BET area (m^2/g)
B2	1.27	16.5	33	1.04	3.43	109
B4	3.71	16	34.7	3.18	3.26	107

2.2. Flow reactor set-up

The experimental set-up is similar to the one described in a previous study [28] except for the addition of a quadrupole mass spectrometer (QMS; MKS Spectra Products; Cirrus LM99), which was used in this study for selected experiments. N_2 was used as the carrier gas before the QMS was installed and was substituted with Ar to monitor N_2 with the QMS. The effluent from the flow reactor was analyzed with a FT-IR spectrometer, quadrupole mass spectrometer, and O_2 analyzer. The species monitored by the FT-IR included NO, NO_2, N_2O, NH_3, and H_2O. The QMS, which sampled the effluent line approximately 0.7 m downstream of the FT-IR, and was calibrated for all of the reactants and products with a minimum of two points. In the current study only N_2 and H_2 concentrations were measured to increase the sampling rate while maintaining high accuracy. For the feeds containing Argon care was taken to ensure that N_2 impurity levels were subtracted from the measured effluent nitrogen data. The time delays for the QMS and FT-IR were estimated and accounted for in the reported temporal data. The reactor temperature was monitored with three type-K stainless steel sheathed thermocouples. A 0.5 mm diameter thermocouple was utilized for the experiments measured the catalyst temperature (T_c) which was positioned within an internal monolith channel at the approximate mid-point of the monolith (radial and axial). The ca. 1 mm gap should provide for a reasonable local temperature even if the thermocouple tip is not in contact with the monolith wall. The gas feed (T_f) and outlet (T_o) temperatures were also monitored by 1/16 in. diameter thermocouples, one 1 cm upstream of the catalyst and the other 1 cm downstream of the catalyst, respectively. Some heat loses occurred from the sample so adiabatic conditions were not achieved.

2.3. Lean and rich cycling experiments

Unless otherwise stated, the lean (storage) feed contained 500 ppm NO and 5% O_2 in N_2 or Ar (60 s) with a total flow rate of 1000 sccm (GHSV = 60,000 h^{-1} based on total monolith volume). Both rich anaerobic (0% O_2) and aerobic (1.5% O_2) feeds were used. The different types of LNT configurations under development may have O_2 in the rich pulse to the LNT, such as diesel applications involving direct injection of fuel into the exhaust or designs in which the diesel oxidation catalyst (DOC) is positioned downstream of the LNT. Designs in which the DOC is upstream of the LNT the rich feed will have little O_2. The cycle-averaged results were obtained over at least 5 cycles after the system had reached a cyclic steady-state. To reach a cyclic steady-state it took approximately 5–20 cycles depending on the conditions but minimally 25 cycles were run at each experimental condition. The total NO_x stored (mol) per lean step was calculated by

$$\mathrm{NO}_x^{\mathrm{stored}}(t_s) = \int_0^{t_s} \left[F^{\circ}_{\mathrm{NO}} - F_{\mathrm{NO}_x}(t)\right] \mathrm{d}t \tag{1}$$

where t_S is the storage time (s), F°_{NO} (mol/s) is the feed rate of NO and F_{NO_x} (mol/s) is the sum of the effluent molar flow rates of NO and NO_2. However, Eq. (1) will slightly over-estimate the amount of NO_x stored at low temperatures because of reaction of N-containing species forming N_2 and N_2O. This is discussed below.

Additional insight about the evolving reaction pathways during the regeneration of stored NO_x with H_2 can be gained by plotting the measured species concentration as a function of the instantaneous stored NO_x conversion which does not include residual stored NO_x (stored NO_x that do not react) and is estimated by the expression

$$[\text{Instantaneous Stored NO}_x\text{ Conversion}]_{t^*} = \frac{\left[\text{Stored NO}_x^{\mathrm{reac}}\right]_{t^*} + \left[\mathrm{NH}_x^{\mathrm{acc}}\right]_{t^*}}{\left[\text{Stored NO}_x^{\mathrm{reac}}\right]_{t^*=t_r} + \left[\mathrm{NH}_x^{\mathrm{acc}}\right]_{t^*=t_r}} \times 100\% \tag{2}$$

where the first term in the numerator in Eq. (2) is the amount of stored NO_x that reacts and is observed in the effluent from the beginning of the regeneration (defined as $t = 0$) until time t^*, and is given by

$$\left[\text{Stored NO}_x^{\mathrm{reac}}\right]_{t^*} = \int_0^{t^*} \left[F_{\mathrm{NH_3}}(t) + F_{\mathrm{NO}_x}(t) + 2(F_{\mathrm{N_2O}}(t) + F_{\mathrm{N_2}}(t))\right] \mathrm{d}t \tag{3a}$$

The second term in the numerator is described below. The denominator in Eq. (2) includes two terms. The first term is the amount of NO_x stored in the previous lean step that reacts during the entire rich pulse of duration t_r and is observed in the effluent. The second term is defined as

$$\left[\mathrm{NH}_x^{\mathrm{acc}}\right]_{t^*=t_r} = \int_0^{t_S} \left[2(F_{\mathrm{N_2O}}(t) + F_{\mathrm{N_2}}(t))\right] \mathrm{d}t \tag{3b}$$

where $x = 0$–3 ($x = 3$ is NH_3). $\left[\mathrm{NH}_x^{\mathrm{acc}}\right]_{t^*=t_r}$ is the amount of NO_x stored that reacts and remains on the catalyst, in the form of adsorbed NH_x species, at the end of the rich pulse. The amount of adsorbed NH_x species is estimated by measuring the amount of N_2 and N_2O produced at the beginning of the subsequent storage step in which feed O_2 primarily reacts with these adsorbed NH_x species to form a mixture of N_2 and N_2O [30] (remark: NO and NO_2 are not important products of ammonia oxidation at temperatures below 300 °C [29]). A more accurate way of estimating $\left[\mathrm{NH}_x^{\mathrm{acc}}\right]_{t^*=t_r}$ is by feeding O_2 in the absence of NO in the subsequent lean step after a cyclic steady-state has been reached [30]. By feeding O_2 devoid of NO in the last lean step eliminates the reaction of NO in the feed with Pt-H (observed to be minimal) and NH_3 (NH_x) which also forms N_2 and N_2O [30]. The sum of $\left[\text{Stored NO}_x^{\mathrm{reac}}\right]_{t^*=t_r}$ and $\left[\mathrm{NH}_x^{\mathrm{acc}}\right]_{t^*=t_r}$ (with NO in the subsequent lean step) is a good estimate of the NO_x^{stored} value with the error less than 6% based on an overall N balance. The value of $\left[\mathrm{NH}_x^{\mathrm{acc}}\right]_{t^*}$ in the numerator of Eq. (2) can only be estimated by additional experiments. This is done by cycling until a cyclic steady-state is reached, then decreasing the final regeneration time, followed by a lean step devoid of NO. The $\left[\mathrm{NH}_x^{\mathrm{acc}}\right]_{t^*}$ term is only important at low temperatures where kinetic limitations are the largest and NH_3 desorption is slow. The results presented in this form show more clearly the evolution of the product distribution as a function of the stored NO_x that reacts. Plots of product concentrations versus time, while instructive, do not convey the differences in NO_x conversion with respect to effluent concentrations for different experiments.

2.4. Rapid pulse experiments

In this set of experiments the regeneration timing was decreased to 3.33 s, consisting of either 4% H_2 or 2.67% NH_3 in

Ar (anaerobic). The duration of the rich pulse was set at 3.33 s as opposed to 3 s because the fastest sampling rate of the FT-IR was 1 Hz. Adding 0.33 s to the regeneration enabled more experimental points to be obtained within the regeneration period by over lapping the last three regeneration steps after a cyclic steady-state was reached (experimental point every 0.33 s). For these experiments, the cycle-averaged data was obtained by averaging over the final 9 cycles after a cyclic steady-state was achieved. When using NH_3 as the reductant all of the feed and effluent lines were heated to 175 °C to minimize NH_3 adsorption on the stainless steel lines, including the switching valve. For this set of experiments only, the NH_3 conversion was calculated by the effluent H_2O concentration instead of NH_3 (=$[NH_{3,in} - 2/3H_2O_{out}]/NH_{3,in}$). The outlet NH_3 concentration was not used because the large concentrations (up to 2.67%) caused errors in the readings by the FT-IR, possibly due to NH_3 adsorbing on the BaF_2 windows.

2.5. Varied catalyst length experiments

The standard catalyst length used in the experiments was 2 cm. Shorter length pieces were obtained by cutting the 2 cm long sample with a diamond saw, or sanding the larger sample if the change in length was very small ($\Delta L < 0.1$ cm). The monolith lengths employed were 1.33, 1.00, 0.67, 0.33, and 0.25 cm. After conducting a series of experiments with the 2 cm long monolith, the sample was removed from the reactor and 0.67 cm was cut off giving a 1.33 cm long piece. The same NSR experiments were then repeated. This approach enabled the "feed" to the last 0.67 cm length of the 2 cm long sample to be determined by measuring the effluent of the 1.33 cm sample. This approach was repeated with several cuts and experiments, enabling the construction of temporal concentration data as a function of monolith length; i.e. temporal concentration profiles. This method, while tedious, avoids any uncertainties caused by sampling gas within a monolith channel with a capillary (Spaci-MS method [19]). An advantage of this method over the simpler variation of the feed flow rate was the maintenance of the same velocity profile in the catalyst. This reduced uncertainties that would have been created due to the variation of the heat and mass transfer coefficients with gas velocity, when the residence time (space velocity) is varied by changing the flow rate.

3. Results

Typical effluent profiles of species present during the storage and regeneration of a 2 cm long $Pt/BaO/Al_2O_3$ (B4) monolith are shown in Fig. 1a–d. In these experiments NO_x was stored for 60 s by contacting the catalyst with a feed gas containing 500 ppm NO contained in 5% O_2 and balance Ar. Then a short, rich pulse of 10 s duration was applied containing 4.3% H_2 and 1.5% O_2 in Ar ($S_{N,p} = (2[O_2] + [NO])/[H_2]) = 0.70$) at a feed temperature of 285 °C. During the storage, very little NO or NO_2 was observed in the effluent during the first 30 s and then a gradual breakthrough of NO and NO_2 was observed (Fig. 1a and c). At the point of rich pulse injection the NO concentration initially increased and then decreased to zero while the NO_2 concentration decreased monotonically towards zero. A rather low concentration of N_2O was observed during the first several seconds, achieving a maximum concentration of about 125 ppm. N_2 appeared within the first second into the pulse and achieved a maximum concentration of about 2100 ppm, after which it began to decrease at about 5 s into the rich pulse. Very shortly after that point NH_3 appeared in the effluent (Fig. 1a and b). A high concentration of H_2 was observed coinciding with the NH_3 breakthrough. Water was observed in the early part of the pulse, and achieved a maximum concentration of about 4% about 6 s into the pulse. A significant

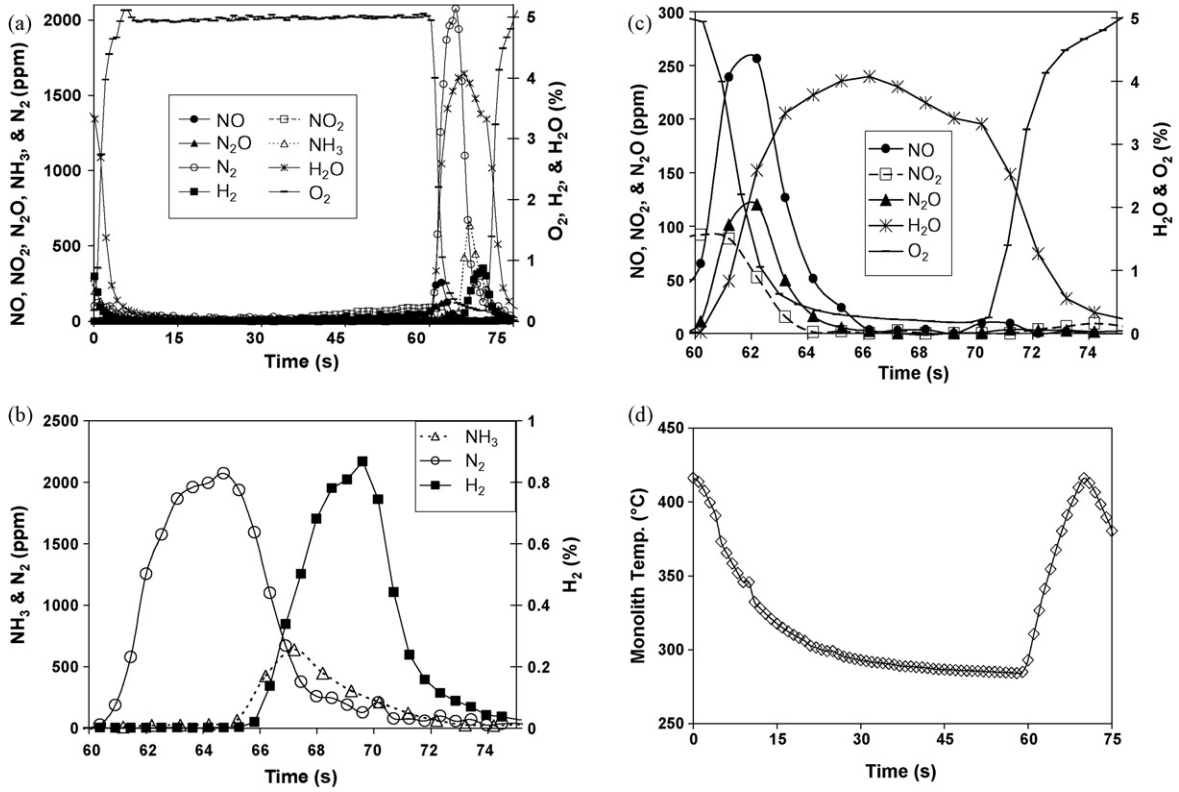

Fig. 1. Effluent profiles of reactants and products at T_f = 285 °C for catalyst B2 (L = 2 cm) (a) N_2, NH_3, NO, NO_2, N_2O, H_2O, and H_2; (b) N_2, NH_3, and H_2; (c) NO, NO_2, N_2O, and H_2O; (d) monolith temperature [lean: 500 ppm NO and 5% O_2 (60 s); rich: 4.3% H_2 and 1.5% O_2 (10 s); $S_{N,p}$ = 0.7].

temperature rise was observed in this experiment (Fig. 1d); the monolith temperature reached a value of about 420 °C near the end of the pulse and then declined slowly to a steady temperature of about 290 °C during the subsequent storage step.

Similar cycling experiments were carried out for a higher loading $Pt/BaO/Al_2O_3$ (B4) monolith. In this set of experiments the effect of monolith length was examined. Fig. 2a and b shows the measured effluent NH_3 concentrations during the regeneration of monolith pieces of four different lengths carried out at two different feed temperatures, 100 and 285 °C. The monolith pieces were obtained from the same original monolith piece of 2 cm length, with three cuts from the back-end to create the 1.33, 0.67, and 0.33 cm long pieces. The rich pulse consisted of 1.5% O_2 and 4.3% H_2 ($S_{N,p} = 0.7$) in both experimental sets. Much higher NH_3 concentrations were observed for the 100 °C feed temperature (up to 3000 ppm) than for the 285 °C feed, which resulted in a maximum NH_3 concentration of only 450 ppm. In both experiments, there was an increase in the time delay before the sharp rise in the effluent ammonia concentration as the length of the monolith was increased, although the increase was much more pronounced at the higher feed temperature. Specifically, for the 100 °C feed the increase in time delay with length, as shown in Fig. 2a, was about 1 s for the 0.33 cm long monolith and about 2 s for the 2.0 cm long monolith. This indicated that ammonia that was produced in the shorter front section, which served as the feed to the next larger section, was largely unaffected. The increase in the ammonia concentration between the smaller and larger pieces indicated that more ammonia was produced. On the other hand, the time delay in the ammonia increase as a function of monolith length was much more pronounced for the 285 °C feed, as shown in Fig. 2b. The 0.33 cm piece ammonia had a delay of about 2 s, but the delay was about 7 s for the 2.0 cm long monolith. An added subtle feature observed for the 285 °C feed experiments was a low but sustained production of ammonia (about 30 ppm; which exceeded the ca. 8 ppm noise level) obtained for all of the monolith pieces prior to the large increase in concentration. This small but non-negligible amount of NH_3 was similarly observed for all of the experiments above 200 °C (not shown here) containing 1.5% O_2 in the regeneration pulse, possibly indicating competitive adsorption between H_2O and NH_3 on Pt.

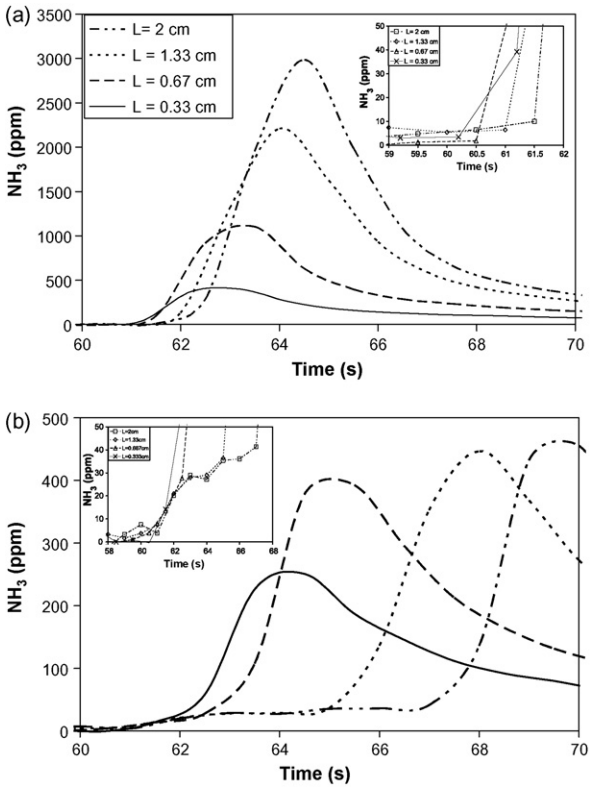

Fig. 2. Effluent NH_3 concentration versus time for varied catalyst (B4) length (a) $T_f = 100$ °C; (b) $T_f = 285$ °C [lean: 500 ppm NO and 5% O_2 (60 s); rich: 4.3% H_2 and 1.5% O_2 (10 s); $S_{N,p} = 0.7$].

The delay in ammonia production with monolith length is clear evidence that ammonia formed upstream either adsorbs or reacts downstream. Since the gas residence time in the full length monolith (2 cm) was only 0.024 s (at 300 °C) any seconds-long delays are clearly an indication of some type of gas–solid interaction. Independent experiments (not shown here) were carried out to determine if the delays were caused by ammonia adsorption on the barium phase or γ-alumina support. These experiments indicated nearly instantaneous appearance of NH_3 in the effluent when a gas containing 400 ppm NH_3 and 1% H_2O in Argon was fed over the BaO/Al_2O_3 monolith catalyst at the same flow rate (1000 sccm) and a range of temperatures (180–470 °C). Above 350 °C the NH_3 effluent profile was nearly identical with and without the monolith piece in the furnace, indicating negligible adsorption. Since ammonia adsorption on Al_2O_3 or BaO is a decreasing function of temperature, the increased delay at higher temperature rules out adsorption as an explanation.

The short, approximately 1 s delay in the appearance of NH_3 for the shortest monolith piece ($L = 0.33$ cm) with the 100 °C feed (Fig. 2a) may be attributed to two factors, kinetic limitations of reaction between adsorbed H_2 and NO on the Pt catalyst in the vicinity of the Barium storage phase and adsorption/desorption of ammonia. The catalytic generation of NH_3 would require the creation of vacant (reduced) Pt sites for spillover of NO and/or the evolution of NO from decomposing nitrites/nitrates. The delay in the large surge in ammonia is comparable at the higher feed temperature (Fig. 2b). This may suggest that ammonia formed upstream reacts with stored NO_x or oxygen that is adsorbed on Pt downstream in the reactor at the start of the regeneration step.

The temperature profiles corresponding to the experiments in Fig. 2a and b are reported in Fig. 3a and b. In these experiments the thermocouple was placed in a center channel at the approximately axial midpoint of each monolith piece. Specifically, for the 2 cm piece the temperature was measured at the 1 cm point, for the 1.33 cm long piece at the 0.67 cm point, and so on. The results show a maximum transient temperature rise of about 160 °C near the front end of the monolith. This compares favorably to the steady-state adiabatic temperature rise for the same feed composition (1.5% O_2 in excess H_2) of about 170 °C. Additional experiments (not shown here) were done to assess the heat effects (back conduction or radiation) by placing the thermocouple approximately 1 mm from the inlet of the monolith in a center channel for the monolith pieces of different lengths for three different feed temperatures ($T_f = 200$, 300, and 400 °C). Those experiments resulted in nearly identical results at a fixed feed temperature, showing that downstream reaction had a negligible effect on the monolith temperature near the entrance for the smaller monolith pieces. These observations reveal that the monolith ignites at the front and the temperature front propagates in the flow direction. Fig. 3 shows that the increase in monolith temperature is independent of the feed temperature (for the same length). This is due to most of the heat generated being from H_2 oxidation, which is nearly independent of the feed temperature.

The cycle-averaged conversions and selectivities from the experiments in Fig. 2a and b are reported in Table 2a and b. (Remark: These values are based on the feed to the reactor and therefore represent integral values.) The NO_x and H_2 conversions

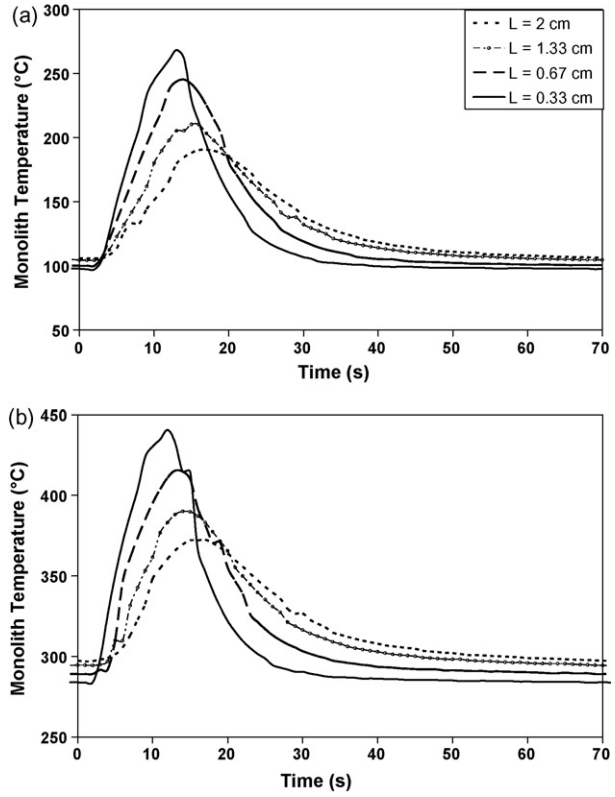

Fig. 3. Monolith temperature profiles for varied catalyst lengths (a) measured in the middle of the monolith, T_f = 100 °C; (b) measured in the middle of the monolith, T_f = 285 °C [lean: 500 ppm NO and 5% O_2 (60 s); rich: 4.3% H_2 and 1.5% O_2 (10 s); $S_{N,p}$ = 0.7].

both increased with monolith length due to the increased NO_x storage on the catalyst for both cases. The N_2 selectivity increased with monolith length for both feed temperatures while the NH_3 selectivity decreased with increasing length at 285 °C. The temporal and spatial evolution of the temperature affects the overall product distribution and must be considered in an interpretation of the results.

Having ruled out simple integral adsorption effects as the only cause for the delay in the appearance in NH_3 in the effluent, the ammonia concentration data reveal both the production and consumption of ammonia. At lower feed temperature (100 °C) the small increase in the appearance of ammonia with incremental length shows increased production of ammonia with minimal consumption/adsorption. The more pronounced increase in the delays encountered at the higher feed temperature (285 °C) clearly suggests that ammonia formed upstream in the monolith is consumed downstream. Following recent studies [26,27], the likely reaction is the reduction of stored NO_x with ammonia. Another possibility is the catalytic reaction of ammonia with molecular oxygen fed during the regeneration or with adsorbed O species on the Pt surface left over from the previous storage step. Either explains the noted consumption of the leading edge of ammonia that is "fed" from one monolith section to the next.

Table 2
Cycle-averaged results for varied catalyst length (B4): (a) T_f = 100 °C; (b) T_f = 285 °C [lean: 500 ppm NO and 5% O_2 (60 s); rich: 4.3% H_2 and 1.5% O_2 (10 s); $S_{N,p}$ = 0.7]

	Monolith length (cm)			
	2	1.33	0.67	0.33
$T_{M,max}$ (°C)	190.9	210.4	245.4	268.2
$T_{M,avg}$ (°C)	131.2	132.5	132.1	128.9
N_2 sel. (%)	13.5	9.6	6.0	2.2
NH_3 sel. (%)	67.0	75.0	78.0	75.6
N_2O sel. (%)	19.5	15.4	16.1	22.2
NO_x conv. (%)	54.5	38.7	20.0	9.5
H_2 conv. (%)	90.4	86.2	79.8	67.1
$T_{M,max}$ (°C)	373.5	390.3	416.2	440.8
$T_{M,avg}$ (°C)	318.4	317.8	314.7	310.0
N_2 sel. (%)	88.5	84.9	73.9	59.7
NH_3 sel. (%)	8.2	11.7	20.8	32.0
N_2O sel. (%)	3.3	3.4	5.3	8.3
NO_x conv. (%)	88.5	67.7	33.6	14.7
H_2 conv. (%)	92.7	88.9	82.8	71.8

Additional varied-length experiments were carried out in which gas phase O_2 was not added during the regeneration step. In these experiments 1500 ppm H_2 (in Ar) was fed for 60 s. This compares to a higher equivalent (excess) H_2 concentration of 1.3% (13,000 ppm) for 10 s in the previous experiments. This experiment allowed for conditions closer to isothermal, a slower reduction process, and a more precise analysis of effluent species concentrations and breakthrough times. Fig. 4a and b shows the typical effluent profiles during this "anaerobic" regeneration. Similar to Fig. 1a and b, the order of nitrogen-containing products appearing in the effluent was N_2O, N_2, and then NH_3. The N_2, N_2O and NH_3 peaks were lower and broader due to the slower feed rate of reductant compared with the earlier aerobic regeneration experiments (Fig. 1). For example, the peak ammonia concentration is lower by a factor of about 2.6. The H_2O concentration was delayed similar to when O_2 was present in the rich pulse. The effluent H_2O concentration approached the inlet feed concentration of H_2 after 10 s of reduction and slowly decayed until the H_2 front reached the exit of the monolith and began to drop off sharply to about 50 ppm. A transient temperature rise of only 7 °C was observed (Fig. 4c), clearly indicating that the heat effects were much less pronounced in this experiment.

The dependence of effluent NH_3 and H_2 on the instantaneous stored NO_x conversion (determined by Eq. (2)) for several different feed temperatures is shown in Fig. 5a and b. In this set of experiments the anaerobic rich pulse contained 1500 ppm H_2. In these data the H_2 and NH_3 break through nearly simultaneously. Moreover, the data show that at lower temperatures ($T < 230$ °C) H_2 and NH_3 break through well before all of the stored NO_x has reacted. At higher temperatures, the little effluent NH_3 that was observed occurred at nearly complete stored NO_x conversion. Similarly, H_2 does not break through until most of the stored NO_x has been converted. These data suggest a rather complicated coupled transient process. The initial NO_x storage values in these data were estimated using Eq. (3a) with $t^* = t_R$ = 60 s and Eq. (3b). Storage estimates are reported in Table 3. During the regeneration (cyclic steady-state), all of the NO_x stored in the previous storage step either reacts or is released forming the "NO_x puff" (NO and NO_2), N_2, N_2O, and NH_3. Once a cyclic steady-state is reached, there is no accumulation over a complete cycle. At higher temperatures (>225 °C) all of the NO_x stored in the previous storage step appears during the subsequent regeneration in the form of unreacted NO and NO_2, or products N_2, N_2O, and NH_3. However, at lower temperatures all of the NO_x stored in the previous storage step does not appear in the form of the aforementioned effluent components by the end of the regeneration. In data to be reported elsewhere [30], at the beginning of the storage step N_2 and N_2O are produced, the concentrations of which decrease with temperature. Their appearance is attributed to oxidation of NH_3 or NH_x species (by O_2 or NO) that has accumulated on the catalyst during the previous regeneration step. The accumulation itself is likely the result of the formation of NH_x or ammonia which desorbs slowly from the catalyst. Taken together, these observations suggest that the observed incomplete conversion of stored NO_x during regeneration

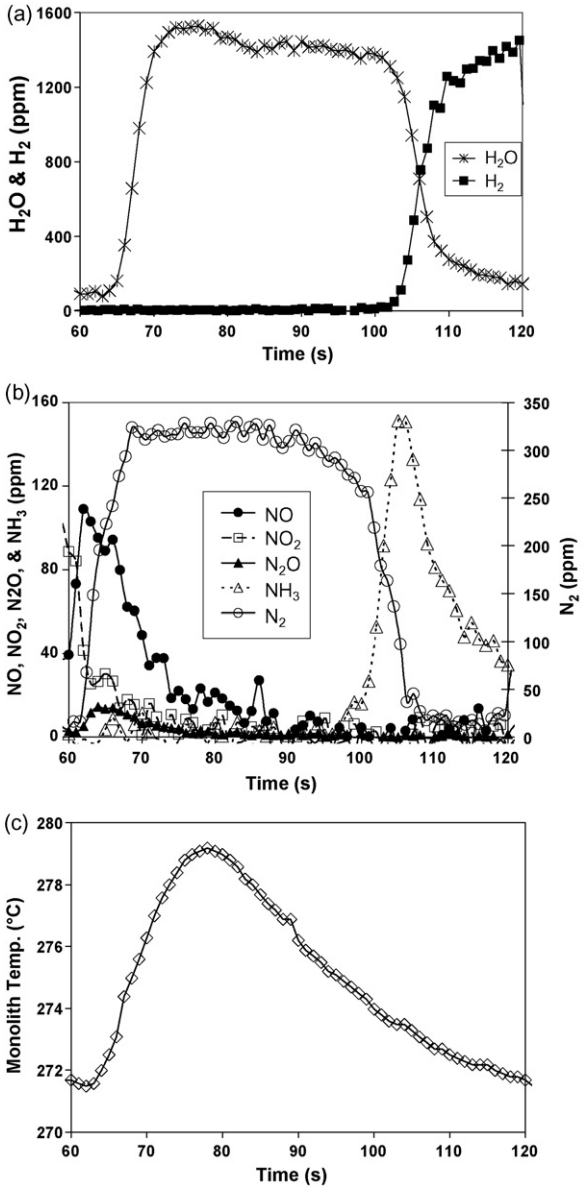

Fig. 4. Effluent profiles of reactants and products at T_f = 275 °C for catalyst B2 (2 cm): (a) H_2 and H_2O; (b) NO, NO_2, N_2O, NH_3, and N_2; (c) monolith temperature [lean: 500 ppm NO and 5% O_2 (60 s); rich: 0.15% H_2 (60 s)].

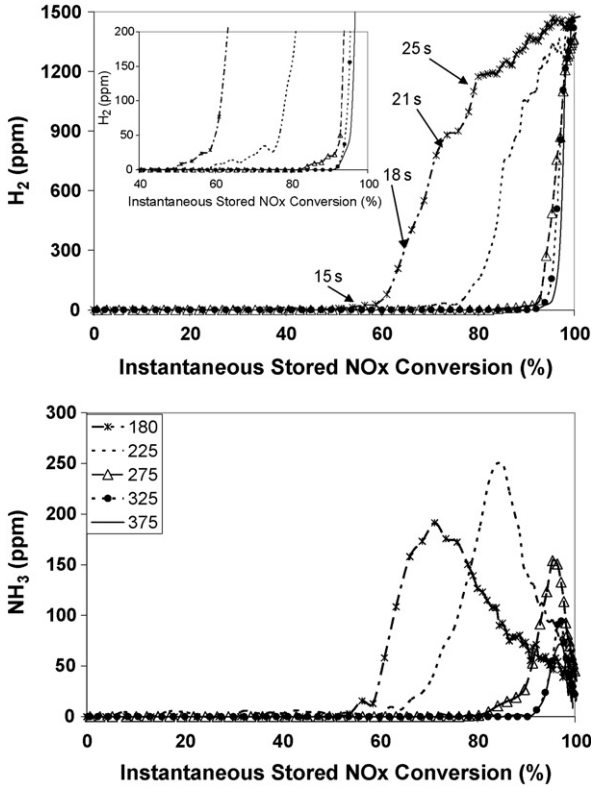

Fig. 5. Effluent concentrations versus NO_x conversion for monolith B2 (L = 2 cm) at T_f = 180 °C–375 °C (a) H_2; (b) NH_3 [lean: 500 ppm NO and 5% O_2 (60 s); rich: 0.15% H_2 (60 s)].

produces accumulated NH_x species which react away during the subsequent storage step.

Having established that ammonia or NH_x accumulation plays a role, the NH_3 adsorption experiments that were conducted on the $Pt/BaO/Al_2O_3$ monolith catalyst, indicate that NH_3 adsorption decreases with increasing temperature, as one would expect. Furthermore, H_2 and H_2O inhibit NH_3 adsorption. These findings suggest that the NH_3 accumulation effect is more important at lower temperatures and in atmospheres containing less water. A good estimate of the amount of NH_3 on the monolith at the end of the regeneration can be made by measuring the amount of N_2 and N_2O formed at the beginning of the lean step. At 180 °C the amount of NH_x species on the catalyst at different times throughout the regeneration was estimated after a cyclic steady-state was reached, and then by varying the duration of the final regeneration step between 10 and 60 s, each followed by a flow of 5% O_2 in Ar. These results are reported in Table 4. The data show that after H_2 breakthrough (at 15 s), the amount of NH_x on the catalyst remains nearly constant. For the single data point prior to breakthrough the accumulated NH_x is less than this level. This suggests that prior to H_2 breakthrough only a portion of the catalyst has been exposed to ammonia.

The dependence of effluent NH_3 and H_2 on the instantaneous stored NO_x conversion is shown for the shorter length B2 catalyst (L = 0.33 cm) at feed temperatures of 180 and 325 °C in Fig. 6a and b. H_2 was observed in the effluent at the onset of the regeneration while NH_3 was slightly delayed at 325 °C (negligible instantaneous stored NO_x conversion, t_R = 1 s). Similarly, at 180 °C H_2 was

Table 3
Moles of NO_x stored, Eqs. (1), (3a), and (3b) estimates, and "NO_x puff" on catalyst B2 (L = 2 cm) at different temperatures [lean: 500 ppm NO and 5% O_2 (60 s); rich: 0.15% H_2 (60 s)]

Temperature (°C)	Eq. (1) NO_x stored (mol × 10^5)	Eq. (3a) (mol × 10^5)	Eq. (3b) (mol × 10^5)	"NO_x puff" (mol × 10^5)	N balance % error
180	1.09	0.89	0.246	0.271	3.57
225	1.68	1.62	0.128	0.196	3.99
275	2.07	2.10	0.036	0.115	3.54
325	2.19	2.24	0.013	0.083	2.95
375	2.22	2.35	0.006	0.170	5.96

Table 4
Estimated moles of NH_x on the catalyst surface at different times during the regeneration of catalyst B2 at $T = 180\ ^\circ C$ ($L = 2.0$ cm) from the moles of N_2 and N_2O formed during the lean without NO

Rich time (s)	N_2 (mol × 10^6)	N_2O (mol × 10^6)	NH_x (mol × 10^6)
60	1.15	0.19	2.67
55	1.16	0.18	2.68
50	1.15	0.19	2.68
45	1.14	0.18	2.64
40	1.18	0.18	2.72
35	1.13	0.18	2.62
30	1.19	0.18	2.75
25	1.11	0.19	2.59
20	1.2	0.19	2.77
15	1.03	0.18	2.41
10	0.87	0.15	2.04

observed instantly when the storage step was switched to the regeneration, while the appearance of NH_3 in the effluent was slightly delayed (approximately at 20% instantaneous stored NO_x conversion). A space velocity effect is undoubtedly the cause for H_2 exiting the reactor at the onset of the regeneration. However the difference in the appearance of NH_3 at 180 and 325 °C (Fig. 6a and b) is presumably due to the slower rate of NH_3 desorption and/or a kinetic limitation at 180 °C, resulting in its appearance in the effluent later than H_2. The results obtained for the 2 cm monolith sample (Fig. 7a and b) show that both H_2 and NH_3 appear in the effluent nearly simultaneously at 180 and 325 °C and at higher instantaneous stored NO_x conversions (approximately 50% at 180 °C and 94% at 325 °C).

Fig. 8a–d shows the effluent concentration profiles of NH_3, N_2, N_2O, and H_2 for six different monolith lengths of catalyst B2 (2.00,

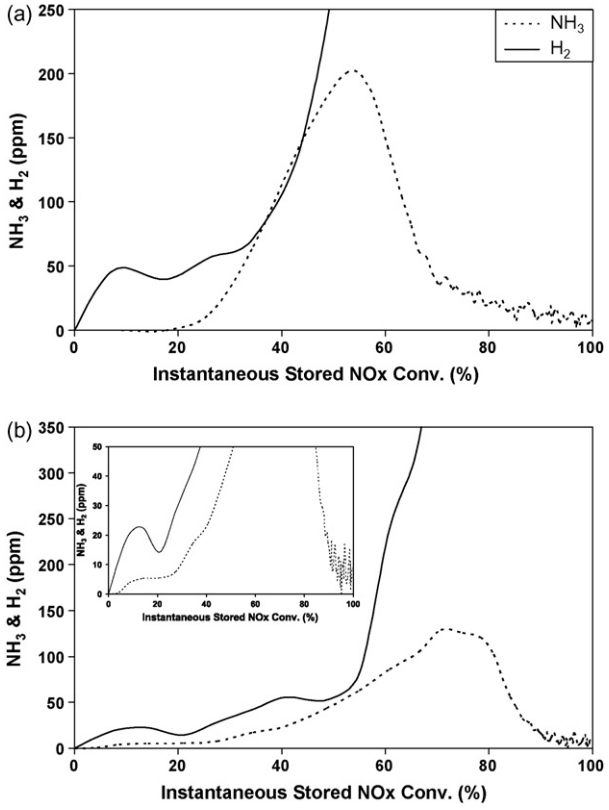

Fig. 6. NH_3 and N_2 effluent concentrations versus NO_x conversion for monolith B2 ($L = 0.33$ cm) at (a) $T_f = 180\ ^\circ C$; (b) $T_f = 325\ ^\circ C$ [lean: 500 ppm NO and 5% O_2 (60 s); rich: 0.15% H_2 (60 s)].

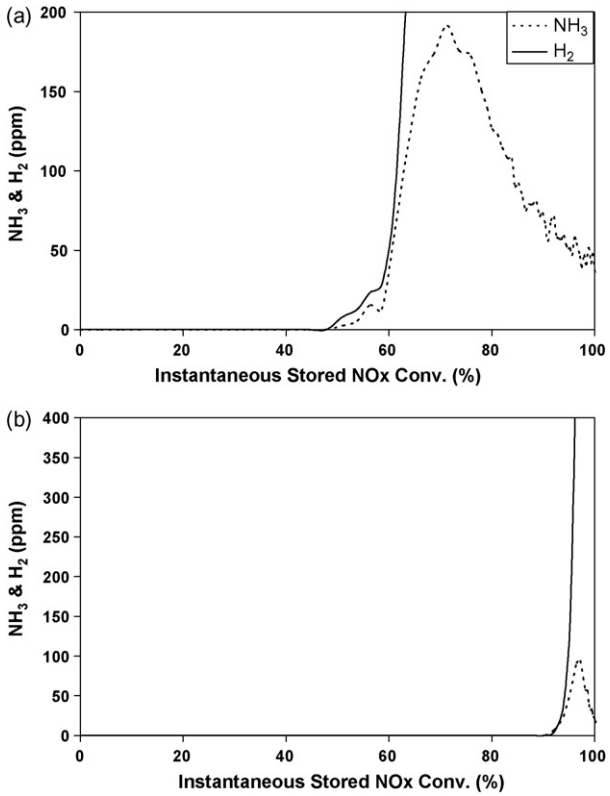

Fig. 7. NH_3 and N_2 effluent concentrations versus NO_x conversion for monolith B2 ($L = 2$ cm) at (a) $T_f = 180\ ^\circ C$; (b) $T_f = 325\ ^\circ C$ [lean: 500 ppm NO and 5% O_2 (60 s); rich: 0.15% H_2 (60 s)].

1.33, 1.00, 0.67, 0.33, 0.25 cm). The lean and rich conditions for this set of experiments were identical to the experiments shown in Fig. 4. The concentrations of N_2 (Fig. 8b) and N_2O (Fig. 8c) both exhibited maxima in their temporal profiles. N_2O has much sharper peaks with increasing length while the peaks in the N_2 concentration broadened with length. For both, the breakthrough delay showed negligible increase with monolith length. These results indicate that the production of N_2 increased with length and once formed, the N_2 exited the reactor. The results for N_2O indicate that it also did not react to a large extent once formed given the lack of any notable delay in its appearance with monolith length. In stark contrast, the NH_3 effluent concentration (Fig. 8a) exhibited pronounced time delays with increasing monolith length as reported in earlier experiments. Again, this is evidence that the ammonia formed upstream reacts downstream. However, unlike the experiments shown in Fig. 4, O_2 was not present during the regeneration, which is evidence that in the current experiments NH_3 reacts with NO_x species supplied by stored nitrites or nitrates. As we discuss later, however, this result does not rule out reaction of ammonia with O_2 in the earlier aerobic pulse experiments. Fig. 8d shows that the time for H_2 breakthrough increased with increasing monolith length, similar to that of NH_3. Once H_2 appeared in the effluent its concentration quickly approached the feed concentration value. For each monolith length, H_2 and NH_3 breakthrough occurred nearly simultaneously.

The corresponding cycle-averaged results of the varied-length anaerobic reduction experiments (0.15% H_2) are shown in Fig. 9. Similar to the aerobic regeneration results (Table 2), the NO_x conversion and N_2 selectivity increased with monolith length, while the NH_3 selectivity decreased with length. These trends coincided with an increase in the NO_x storage (Table 5). This reaffirms the mechanism that stored NO_x reacts with H_2 in the feed

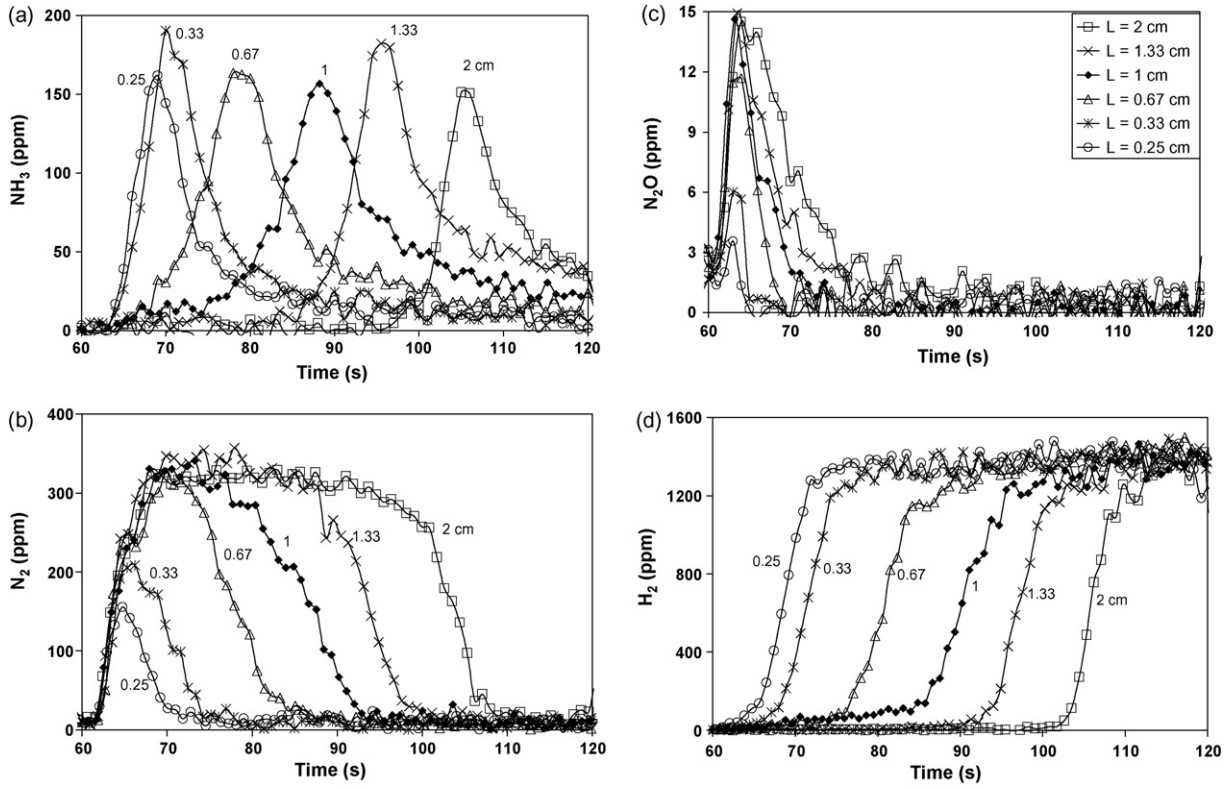

Fig. 8. Effluent concentrations for varied monolith length (B2) at T_f = 275 °C (a) NH_3; (b) N_2; (c) N_2O; (d) H_2 [lean: 500 ppm NO and 5% O_2 (60 s); rich: 0.15% H_2 (60 s)].

and intermediate NH_3 along the monolith, leading to an increase in the NO_x conversion and N_2 selectivity. The decrease in ammonia selectivity is consistent with its reaction with stored NO_x downstream of its production zone. The N_2O selectivity is minimal due to the moderate temperature. The cycle-averaged NO_x conversion (Fig. 9) increased from 22 to 87% for the shortest (0.33 cm) to longest monolith piece (2 cm). The low conversion for the shortest piece is due to leakage of NO_x during the 60 s storage step.

The cycle-averaged NO_x conversion and product selectivities as a function of monolith temperature are reported in Fig. 10a for the longest monolith piece (2 cm). The NO_x conversion increased monotonically with temperature, corresponding to increased NO_x storage with temperature (reported in Table 3). The N_2 selectivity also increased with temperature while the selectivity to N_2O and NH_3 decreased. The dependence of the calculated cycle-averaged moles (yield) of N_2, NH_3, and N_2O on the monolith temperature are shown in Fig. 10b. These values were obtained by integrating the corresponding molar flow rates over a complete cycle. Most of the trends in the amounts of N_2, NH_3, and N_2O are similar to their selectivity trends. One exception is the result for NH_3 which shows a maximum in the yield of ammonia at 225 °C.

From the temporal data, the evolution of the spatially propagating fronts of hydrogen and ammonia can be constructed in the form of concentration versus length plots at fixed times. This was done by defining a reference point for the H_2 and NH_3 concentration versus time plots. For H_2 we used the point at which the hydrogen concentration was at 50% of its feed value (750 ppm) while for NH_3 we used the peak ammonia concentration. The speeds of the propagating fronts were estimated by measuring the ratio of the change in position of the reference point with change in time.

The results of the traveling front construction are provided in Fig. 11a and b (concentration versus distance) and Table 6 (front velocity). The H_2 concentration at the inlet of the monolith (feed) was at its 1500 ppm feed value, and decreased sharply to zero at the beginning of the regeneration. As the regeneration proceeded the H_2 front moved down the length of the reactor. The sharp decrease in the H_2 concentration is presumably due to the

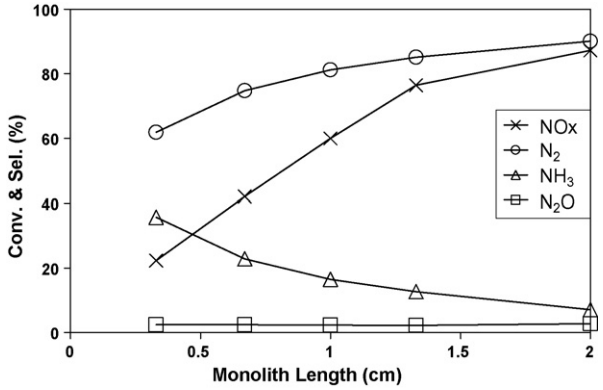

Fig. 9. Cycle-average NO_x conversion and N_2O, N_2 and NH_3 selectivities for catalyst B2 (T_M = 275 °C) [lean: 500 ppm NO and 5% O_2 (60 s); rich: 0.15% (60 s)].

Table 5
Moles of NO_x stored and moles of NO_x stored per cm of monolith on catalyst B2 at T = 275 °C for several monolith pieces of different length [lean: 500 ppm NO and 5% O_2 (60 s); rich: 0.15% H_2 (60 s)]

L (cm)	NO_x stored (mol × 10^5)	NO_x stored per cm of monolith (mol/cm × 10^5)
0.33	0.57	1.73
0.67	1.02	1.52
1	1.42	1.42
1.33	1.78	1.34
2	2.07	1.04

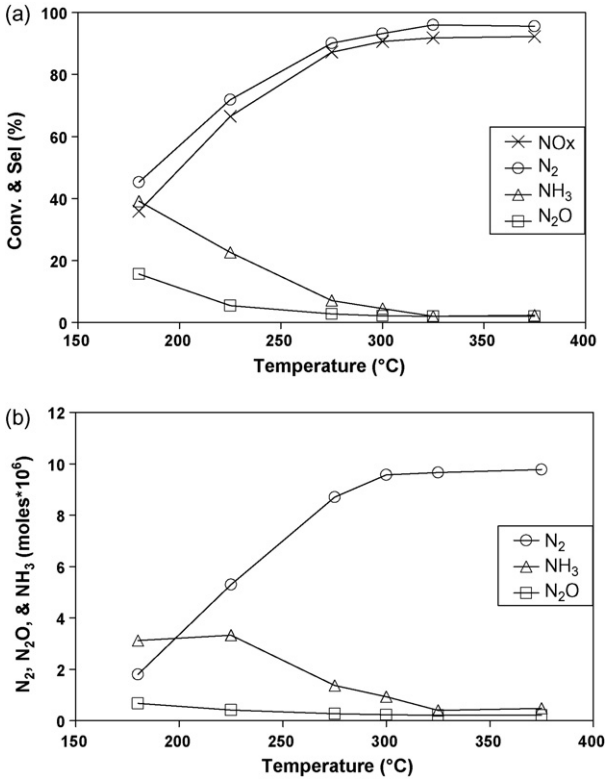

Fig. 10. Cycle-average results for catalyst B2 (a) NO_x conversion and N_2O, N_2 and NH_3 selectivities (L = 2.00 cm); (b) production of N_2, N_2O, and NH_3 (L = 0.2 cm) [lean: 500 ppm NO and 5% O_2 (60 s); rich: 0.15% (60 s)].

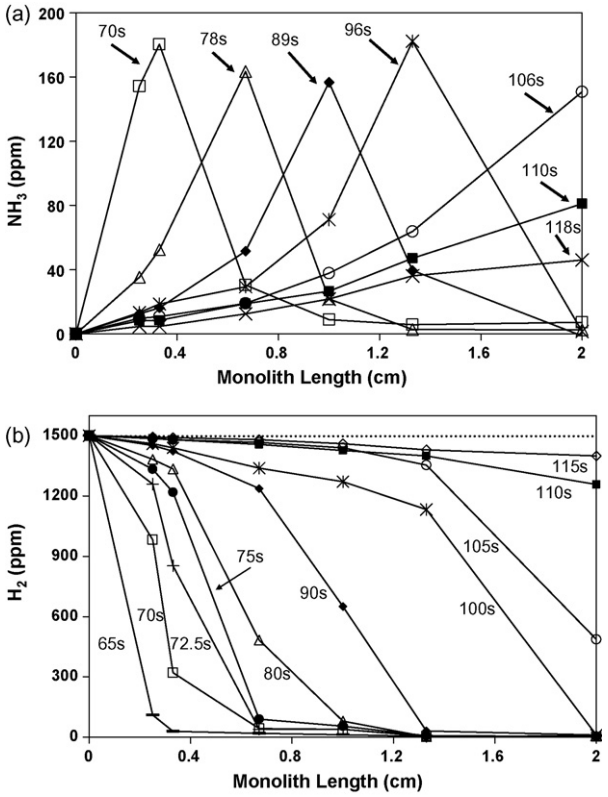

Fig. 11. Effluent concentration versus length at T_c = 275 °C (a) NH_3; (b) H_2 [lean: 500 ppm NO and 5% O_2 (60 s); rich: 0.15% H_2 (60 s)].

consumption of H_2 first by oxygen adsorbed on Pt and then by reaction with stored NO_x, forming a mixture of N_2, N_2O, and NH_3. On the other hand, the NH_3 "front" is actually a moving pulse since NH_3 is formed and consumed. The temporal traveling front data reveal that the H_2 front accelerated as it propagated down the length of the monolith. These results are analyzed in the next section.

The effect of H_2 concentration on the NO_x trap regeneration dynamics was examined. Fig. 12a and b are additional varied-length experiments for anaerobic pulses containing different feed concentrations of H_2. The regeneration consisted of 1% H_2 (Fig. 12a) and 0.3% H_2 (Fig. 12b) for a duration of 60 and 30 s, respectively. The regeneration times and small amounts of reductant fed (0.3% H_2) were not optimal but were implemented in order to monitor NH_3 formation over a longer period of time for analysis purposes. The NH_3 effluent profiles were observed to increase in steepness as the amount of H_2 fed was increased. Due to an increased supply rate of H_2, the regeneration of the NO_x trap was accomplished in a shorter amount of time than reported in earlier experiments. As before, the measured NH_3 in the effluent was delayed in the order of smallest to largest monolith length.

More realistic cyclic NO_x storage and reduction experiments comprising short pulses of 3.33 s duration were studied in order to compare NH_3 and H_2 as reductants (Fig. 13). The regeneration time was decreased to 3.33 s with 4% H_2 or 2.67% NH_3 in the absence of O_2. (These concentrations gave the same 8% feed of H atoms.) The cycle-averaged results for NO_x conversion show that the H_2 feed resulted in greater than 60% conversion over the entire temperature range while for the NH_3 feed the NO_x conversion was as low as 5% at 130 °C and increased above 60% when the temperature exceeded 230 °C. Unlike NH_3, H_2 was able to sustain >60% reductant conversion at rather low temperatures (as low as 130 °C). Similar to the cycle-averaged NO_x conversion trend with NH_3 as the reductant, the cycle-averaged NH_3 conversion was low (< 20%) below 180 °C and then increased to 60% at 230 °C. The increase in conversion coincided with the light-off temperature of NH_3 oxidation (about 180 °C) [29]. As the temperature increased the NO_x conversions obtained with H_2 and NH_3 converged and were nearly equal at 400 °C. Similarly, the H_2 and NH_3 conversions converged as the temperature was increased and were nearly identical at 400 °C. Two experimental points were repeated, one at 230 °C with NH_3 as the reductant and the other at 330 °C with H_2 as the reductant. These two points were repeated to determine the reproducibility for this set of experiments. All four experimental points were within 2% of the original experiments.

4. Analysis and discussion

The experimental results suggest the following reaction network depicted in Fig. 14. The network has a triangular structure

Table 6
Estimated speed of H_2 and NH_3 fronts in different sections along the monolith length at T_f = 275 °C for catalyst B2 [lean: 500 ppm NO and 5% O_2 (60 s); rich: 0.15% H_2 (60 s)]

Location along the monolith (cm)	Incremental length (cm)	Velocity (mm/s)	
		H_2	NH_3
0–0.25	0.25	0.29	0.28
0.25–0.33	0.08	0.31	0.33
0.33–0.67	0.33	0.35	0.37
0.67–1	0.33	0.40	0.38
1–1.33	0.33	0.47	0.45
1.33–2	0.67	0.79	0.74

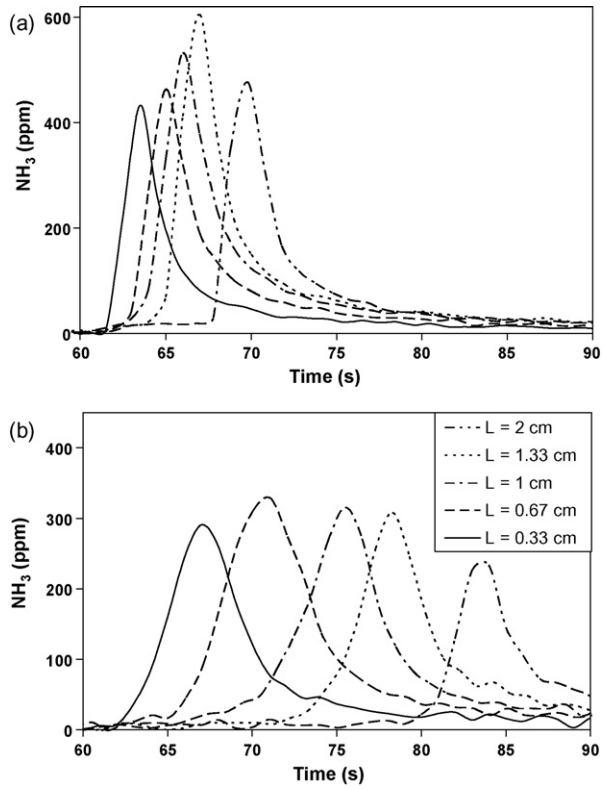

Fig. 12. NH_3 effluent concentration vs. time for varied catalyst (B2) length at 325 °C; (a) 1% H_2; (b) 0.3% H_2 [lean: 500 ppm NO and 5% O_2 (60 s); rich: 1% H_2 (60 s) or 0.3% H_2 (30 s)].

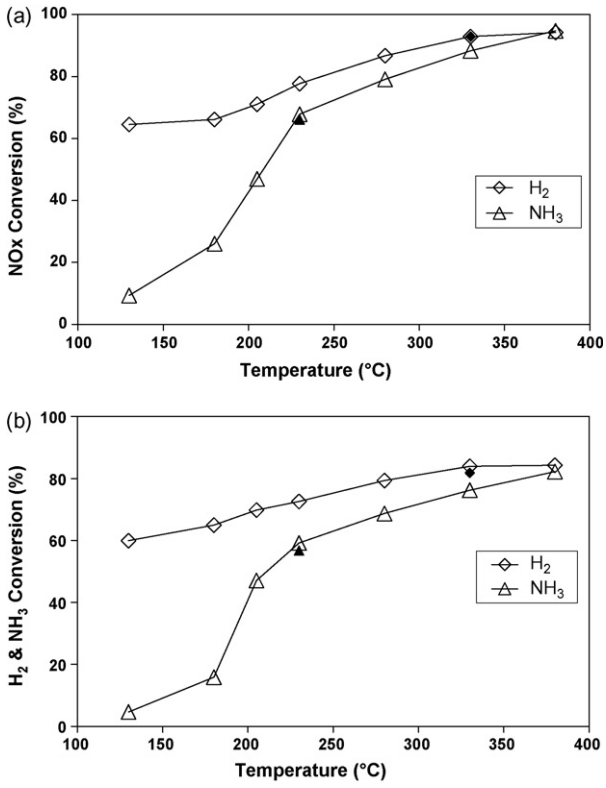

Fig. 13. Cycle-average results for catalyst B2 (a) H_2 and NH_3 conversion; (b) NO_x conversion [lean: 500 ppm NO and 5% O_2 (60 s); rich: 4% H_2 or 2.67% NH_3 (3.33 s)].

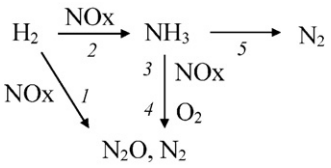

Fig. 14. Simplified reaction network showing the conversion of reductant H_2 and stored NO_x to nitrogen-containing products N_2O, N_2, and NH_3.

comprising five paths to the N-containing products N_2O, N_2, and NH_3 that occur during the regeneration of the lean NO_x trap with H_2 as the reductant:

- *Path 1* is the reaction between reductant H_2 and stored NO_x to mostly N_2 (and some N_2O); The overall stoichiometry for this path is $Ba(NO_3)_2 + 5H_2 \xrightarrow{Pt} N_2 + BaO + 5H_2O$
- *Path 2* is the reaction between reductant H_2 and stored NO_x to NH_3; The overall stoichiometry for this path is $Ba(NO_3)_2 + 8H_2 \xrightarrow{Pt} 2NH_3 + BaO + 5H_2O$
- *Path 3* is the reaction between stored NO_x and NH_3, acting as an intermediate reductant, to mostly N_2 (and some N_2O); The overall stoichiometry for this path is $Ba(NO_3)_2 + 10/3NH_3 \xrightarrow{Pt} 8/3N_2 + BaO + 5H_2O$
- *Path 4* is the reaction between O_2 and NH_3 to N_2O and N_2; With reaction stoichiometry as follows $NH_3 + 3/4O_2 \xrightarrow{Pt} 1/2N_2 + 3/2H_2O$
- *Path 5* is the decomposition of NH_3 to N_2 and H_2; $2NH_3 \xrightarrow{Pt} N_2 + 3H_2$

N_2 is the product of four different combinations of these paths. The first is by the direct reduction of NO_x by hydrogen (path 1); the second is by the sequential formation and consumption of NH_3, H_2 reduction of stored NO_x followed by NH_3 reduction of additional stored NO_x (path 2/3); the third is by sequential formation and consumption of NH_3, in this case by NH_3 oxidation (path 2/4); and the fourth is by the sequential reduction of NO_x by H_2 to NH_3 followed by its decomposition (path 2/5). As we describe below, the extent of each route is a complex function of the local conditions in the reactor, including temperature, gas phase and surface compositions.

When the pulse contains gas phase O_2 the hydrogen oxidation reaction evolves considerable heat which is important at low temperatures in overcoming energy barriers. The rich pulse containing 1.5% O_2 and 4.3% H_2 results in a transient temperature rise of about 150 °C.(Fig. 3a and b). The scavenging of oxygen adatoms by hydrogen creates empty Pt sites, which provide a route for decomposition of barium nitrites and nitrates in close proximity; these are the so-called "proximal" storage sites. Medhekar et al. [18] showed in H_2 - NO pump/probe TAP experiments that this interfacial chemistry occurs under isothermal conditions. The extent of NO conversion to N_2O and N_2 depends on the availability of vacant sites created by the scavenging of oxygen by hydrogen. The selectivities to N_2O and N_2 are dictated by the temperature and coverages of O, N and NO species. The existence of this mechanism does not preclude an alternative route involving the spillover of activated reductant adsorbed on Pt onto proximal barium nitrite/nitrate species where partial reduction of stored NO_x occurs releasing NO [7]. As shown previously, Pt is also an excellent catalyst for ammonia production [28,29]. Once the Pt surface has been cleaned of oxygen, the reaction of surface H and N (from NO dissociation) may occur, forming NH_3. The extent of ammonia production depends on the temperature and the H/N surface coverage ratio.

Additional chemistries that complicate the situation include catalyzed ammonia oxidation (path 4) and ammonia decomposition (path 5). Clayton et al. [29] have shown that Pt/BaO is an excellent catalyst for ammonia oxidation, with products N_2, N_2O, NO, and NO_2 with selectivities determined by the NH_3/O_2 ratio and catalyst temperature. The ignition/light-off temperature of NH_3 with O_2 is about 180–200 °C [29]. In the 100 °C feed temperature experiments involving the aerobic pulse a large temperature spike increased the monolith temperature well above the light-off temperature for NH_3 oxidation, enabling NH_3 to react further. In the same study Clayton et al. [29] showed that ammonia decomposition occurs at temperatures exceeding 350 °C. However, small concentrations of H_2 inhibit NH_3 decomposition, therefore making path 5 secondary upstream and within the H_2 front, where the H_2 concentration is non-negligible. Moreover, at the leading edge of the H_2 front NH_3 decomposition will also be a secondary route due to a Pt surface that is predominantly covered by NO and O adatoms. In addition, the conditions of a regeneration feed devoid of O_2 makes path 4 a contributing route during the regeneration only at the leading edge of the ammonia pulse. Moreover, as discussed above, accumulated ammonia species will react with oxygen during the beginning of the storage step.

The data in this study conclusively reveal that ammonia produced in the LNT can serve as a reductant of stored NO_x, supporting recent studies [26,27]. The production of ammonia by the aforementioned chemistry implies the existence of adsorbed NH_3 or its precursors (NH_x). These species are potential reductants of unreacted NO_x. The scenario involves the upstream production of ammonia by reaction of NO and H_2 on Pt, followed by the desorption and subsequent downstream reduction of stored NO_x by NH_3. The steps involving the latter involve the readsorption of NH_3 on Pt, followed by either reaction of NH_3 and NH_x species with oxygen or dehydrogenation. The production of surface hydrogen species enables the scavenging of surface oxygen, freeing up sites for proximal stored NO_x to spillover and dissociate and gaseous NO to adsorb and dissociate. A less likely route is the direct reaction of NH_3 with barium nitrites and nitrates. Nova et al. [11] have shown that reaction between gas phase H_2 and $Ba(NO_3)_2$ does not occur, and therefore $Ba(NO_3)_2$ must first decompose before reaction with H_2 occurs. Cycling experiments conducted at 400 °C with NH_3 (rich) and NO_2 (lean) exposed to the Pt-free BaO monolith catalyst, indicating activity. However, the activity was notably lower than the catalyst containing Pt.

With the role of ammonia as a hydrogen carrier and reductant confirmed, a mechanistic question to resolve is what are the relative extents of stored NO_x reduction by H_2 (path 1) and NH_3 (path 2/3). On the one hand, N_2 appears at the onset of the regeneration, well before NH_3 in all of the experiments. For example, results with the 2 cm monolith at a feed temperature of 275 °C and prolonged pulse of 60 s (Fig. 8a and b) show significant N_2 production during the first part of the regeneration and NH_3 towards the end of the regeneration when the instantaneous stored NO_x conversion is greater than 90% (Fig. 5a and b). One interpretation of these data is that NH_3 is formed more slowly than N_2, hence its later appearance in the effluent. On the other hand, Clayton et al. [29] showed the N_2 and NH_3 selectivities are dictated by the NO/H_2 feed ratio; for $NO/H_2 \geq 1$, mainly N_2 is favored, for $1 \leq NO/H_2 \leq 0.4$ both N_2 and NH_3 are formed while for $NO/H_2 < 0.4$ mostly NH_3 is formed. Extending this argument to transient conditions, the local NO/H_2 ratio will dictate the transient product selectivity. At the leading edge of the H_2 front, N_2 will be formed because of the accumulated NO and O adatoms on Pt and stored NO_x. As these adsorbed species are reacted away the selectivity will shift to ammonia. As the H_2 front approaches the end of the monolith the N_2 production drops off with NH_3 breakthrough occurring and its formation taking over. Evidence for ammonia formation follows from the shorter monolith sections experiments that clearly reveal its production at the front part of the monolith at the beginning of the regeneration (Fig. 6a). Experiments with shorter and richer regeneration expose the kinetic differences between H_2 and NH_3 (Fig. 13). The direct route to N_2 is favorable at low temperatures for shorter and richer regenerations, as we discuss below.

The transient concentration data of this study reveal the existence of NH_3 and H_2 in the effluent stream. In fact, the breakthrough of NH_3 and unreacted H_2 occur nearly simultaneously. Clayton et al. [29] showed H_2 to be a more effective reductant than NH_3 during the steady-state reduction of NO by a mixture containing NH_3 and H_2. These steady-state findings suggest that the production of H-Pt and/or NH_x-Pt species from NH_3 may be slower than H-Pt production from H_2. However, it is difficult to conclusively determine if a similar process applies under conditions in which the supply of NO_x is from the solid barium nitrites/nitrates as opposed to the gas phase (NO). Moreover, the spatial and temporal resolution required to quantify the moving hydrogen and ammonia concentration fronts precludes the establishment of a definitive mechanism. Following the arguments put forth by Pihl et al. [26] and Cumaranatunge et al. [27], the ammonia front may slightly lead the hydrogen front, enabling ammonia to catalytically react with NO_x species supplied from proximal NO_x storage sites and from oxygen adatoms on Pt.

The rapid pulse cycling experiments directly comparing H_2 and NH_3 over a range of temperatures expose their differences in reduction reactivity (Fig. 13). Comparable cycle-averaged NO_x and reductant conversions (<10% difference) were obtained when using H_2 and NH_3 as reductants for feed temperature exceeding 280 °C. H_2 was slightly more efficient in reducing stored NO_x up to 380 °C. On the other hand, for temperatures below 230 °C NH_3 was much less effective than H_2 in reducing stored NO_x. The temperature demarcation for which the drop in ammonia conversion was observed is consistent with the light-off temperature of NH_3 oxidation (180–200 °C). This may suggest that the rate limiting step for NO_x reduction by NH_3 is the same one as for the Pt catalyzed oxidation of NH_3; possibilities include the decomposition of adsorbed NH_3 into NH_x adspecies or their oxidation by O–Pt or NO–Pt.

The estimation of the velocities of the H_2 and NH_3 fronts helps to elucidate the rate limiting step during the regeneration of the NO_x trap. Cumaranatunge et al. [27] suggested that the reduction step is limited by mass transfer of the gas phase reductant to the catalyst surface since the reduction process was observed to be equally effective when using H_2 or NH_3 as the reductant while keeping the same feed rate of H atoms. Our experimental findings show that the regeneration is initially feed rate limited based on the complete absence of the reductant in the effluent during the first part of the regeneration. Moreover, our results concur that there is a small difference between H_2 and NH_3 as long as the temperature exceeds about 380 °C. In the absence of stored NO_x the H_2 front velocity would equal the gas velocity (i.e. negligible amount of H_2 adsorption compared to the amount fed). However, the estimated front velocities, 0.02–0.08 cm/s, are considerably slower than the linear velocity of the feed gas, which is approximately 115 cm/s for the 1000 sccm feed rate at 300 °C. During the period in which H_2 is completely consumed (i.e. no H_2 in the effluent) the H_2 propagation is therefore limited by the consumption of H_2 as it reduces the stored NO_x. This is a so-called "feed-limited" state. As the regeneration proceeds, H_2 eventually breaks through, and the rate limiting step is no longer the supply of H_2.

The traveling front velocity of H_2 or of the leading edge of NH_3 depends on the amount of NO_x stored. The data indicate that the H_2

Table 7
Estimated moles of stored NO_x in different sections of the monolith B2 at $T = 275$ °C

ΔL (cm)	NO_x stored (mol × 10^6)	NO_x stored per cm of monolith (mol/cm × 10^6)
0–0.33	5.71	17.3
0.33–0.67	4.47	13.5
0.67–1.0	4.06	12.3
1.0–1.33	3.60	10.9
1.33–2.0	2.82	4.2

front accelerates down the length of the monolith (Table 6, Fig. 11b). The simplest explanation is that more NO_x is stored at the front part of the monolith, hence more H_2 is needed to reduce the stored NO_x. Note that in these experiments the trap was sufficiently regenerated by prolonged rich feeds. The amount of NO_x stored in an incremental length of monolith can be estimated from the expression

$$NO_x^{stored}(\Delta L) = NO_x^{stored}(L_2) - NO_x^{stored}(L_1) \quad (4)$$

Using this formula, the NO_x storage was determined to decrease from the front end to the back end of the monolith (Table 7). As a result, the hydrogen front accelerated as it was exposed to lower amounts of stored NO_x, as expected.

The data indicate that the velocity of the H_2 and NH_3 fronts are not only dependent on the amount of stored NO_x, but also on the temperature, stoichiometric number of the pulse ($S_{N,p}$), and H_2 feed concentration during the regeneration. When the concentration of reductant was increased the NH_3 front velocity increased, the results of which are reported in Table 8 for 0.15%, 0.3%, and 1% H_2 feeds.

A quantitative analysis of the traveling front velocity helps to elucidate the main variables affecting the overall rate of regeneration. In a reductant feed-limited state, the front velocity, v_f, scales with the ratio of the stored NO_x/reductant feed rate (for an anaerobic feed). Expressions for estimating the H_2 front velocity is given by

$$v_f = \frac{F^o_{H_2}\,\Delta L}{(NO_x^{stored}(L_2) - NO_x^{stored}(L_1))\upsilon}, \qquad v_f = \bar{u}\left(\frac{R_\Omega}{\delta_c}\right)\left(\frac{C^o_{H_2}}{S^o_{NO_x}\upsilon}\right) \quad (5)$$

where $NO_x^{stored}(z)$ is the NO_x storage as a function of length (it was previously defined in the experimental section with the values reported in Table 7), υ is the reduction stoichiometry (mol H_2 reacted/mol NO_x reacted) and ΔL ($=L_2 - L_1$) is the length of the section of the monolith piece considered. In Eq. (5) R_Ω is the channel hydraulic radius, δ_c is the washcoat thickness and $S^o_{NO_x}$ is the amount of NO_x stored per unit volume of washcoat. Eq. (5) assumes that all of the H_2 reacts with stored NO_x and that the reaction with oxygen adatoms on the Pt crystallites left over from the previously storage step is negligible. If we assume that NO_x is stored as barium nitrate and that reduction gives BaO, N_2 and H_2O as products, we have:

$$Ba(NO_3)_2 + 5H_2 \xrightarrow{Pt} N_2 + BaO + 5H_2O$$

so that $\upsilon = 2.5$. Under feed-rate limited conditions the temperature expectedly has a negligible effect on the estimated velocity. However, the ratio of nitrites/nitrates will affect the velocity of the moving fronts since $\upsilon = 1.5$ for the reduction of $Ba(NO_2)_2$. Therefore, this method slightly under estimates the front velocity since NO_x stored as nitrites are not considered. Taking $R_\Omega = 250$ μm, $\delta_c = 25$ μm, $C^o_{H_2} = 1500$ ppm, and $S^o_{NO_x} = 0.5$ mol/L washcoat ($T = 275$ °C) gives $v_f = 0.3$ mm/s which is close to the experimental value (Table 6). As stated earlier this is a theoretical lower bound on the velocity. A higher velocity will be observed if there are any kinetic limitations during reduction or if the NO_x is not all stored as nitrates.

A more detailed estimate of the reductant front velocity can be obtained by utilizing the product distribution data. Over an incremental length of monolith (ΔL) the front velocity satisfies

$$v_f = \frac{\Delta L}{t^*}, \quad (6a)$$

where t^* is the time required for the reductant to react with all of the stored NO_x species in that section of monolith. If we assume that H_2 is the reductant, t^* is estimated by

$$t^* = \frac{\int_0^{t_{S+R}} (F_{H_2O}(t) + 1.5F_{NH_3}(t))\,dt}{F^o_{H_2}} = \frac{\int_0^{t_{S+R}} (F^o_{H_2}(t) - F_{H_2}(t))\,dt}{F^o_{H_2}} \quad (6b)$$

Here F_{H_2O} and F_{NH_3} are the measured effluent molar flow rates of reduction products H_2O and NH_3, $F^o_{H_2}$ is the molar feed rate of H_2 and t_{S+R} is the time of one complete lean and rich step. This analysis assumes that there is a discontinuity in the effluent H_2 from zero concentration to its feed value precisely at t^*. On the other hand, the experiments indicated that the H_2 effluent profile had a sigmoidal shape, rather than a step-like transition. The sigmoid suggests that the rate limiting step of the regeneration of the trap switches from the supply of H_2 to another rate limiting step. We carried out H_2 pulsing experiments which showed a much sharper transition in the absence of stored NO_x. We return to this issue below.

The values in Table 6 were compared to the values estimated by Eqs. (5), (6a) and (6b) for the average front velocity and are shown in Fig. 15. The measured values ($\Delta L/\Delta t$) and calculated ones (Eqs. (5), (6a) and (6b)) are in good agreement except for the last 0.67 cm of the monolith where the estimated value (Eq. (5)) exceeds the measured values. This may be due to NO_x released

Table 8
Estimated average velocity of NH_3 front as a function of temperature and H_2 concentration for catalyst B2 ($L = 2$ cm) [lean: 500 ppm NO and 5% O_2 (60 s); rich: 1% H_2 (60 s), 0.3% H_2 (30 s), and 0.15% H_2 (60 s)]

Feed temperature (°C)	Average velocity of NH_3 front (mm/s)		
	1% H_2	0.3% H_2	0.15% H_2
180	3.2	1.6	1.0
225	2.8	1.1	0.58
275	2.2	0.90	0.44
300	–	0.88	0.42
325	2.1	0.85	0.42
375	2.0	0.87	0.40

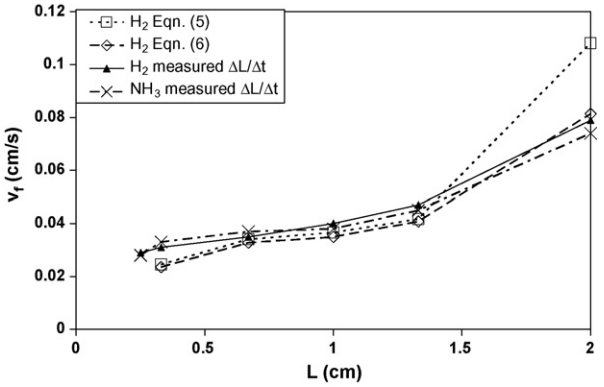

Fig. 15. Velocity of fronts measured and calculated for varied monolith length (B2) at $T_f = 275$ °C [lean: 500 ppm NO and 5% O_2 (60 s); rich: 0.15% H_2 (60 s)].

upstream (0–1.33 cm section) of the last 0.67 cm of the monolith during the initial portion of the regeneration, which is then stored in the last 0.67 cm. Table 7 shows that the amount of NO_x stored per cm of monolith is much lower in the last 0.67 cm than the other portions of the monolith. Therefore, the estimate for the amount of NO_x stored (Eq. (1)) near the exit (last 0.67 cm of monolith) is less than the amount of NO_x that reacts in the last section, causing the estimate for Eq. (5) to over-estimate the velocity of the H_2 front.

Identification of the rate limiting processes is key to optimizing the lean NO_x trap. As described above, H_2 and NH_3 breakthrough occur when the supply of H_2 is no longer the rate limiting process. As mentioned earlier, under some conditions, most notably at lower temperatures (<230 °C), H_2 and NH_3 breakthrough occurred at intermediate NO_x conversions (Fig. 5a and b). On the other hand, steady-state experiments of the NO + H_2 on Pt/BaO reaction system carried out by Clayton et al. [29] showed that under conditions similar to those in Fig. 5 (i.e. space velocity, Pt loading and dispersion, temperature, feed concentration) the reduction of NO by H_2 led to complete conversion of the limiting reactant. Similar to these steady-state results, the cycling results never showed NO_x and H_2 (or NH_3) in the effluent simultaneously, indicating that the supply of the reactant not observed in the effluent (reductant or NO_x) was rate limiting. Thus, the appearance of H_2 and/or NH_3 in the effluent at intermediate NO_x conversion suggests that the transport of stored NO_x to Pt is the likely bottleneck. Unlike the steady-state experiments, the supply of NO_x comes from the storage phase, not the feed, and likely occurs in the vicinity of the Pt/BaO interface. The likely steps involved include stored NO_x decomposition and spillover to Pt and/or spillover of hydrogen to the barium phase [14–17]. At the beginning of the regeneration phase the "proximal" nitrites/nitrates are locally depleted and as reaction proceeds the NO_x supply must come from NO_x stored further from the Pt/BaO interface. Muncrief et al. [10] described a phenomenological picture using propylene as a reductant. That picture proposed that a diffusional limitation of NO_x through the barium phase limited the regeneration rate. Tuttlies and Eigenberger [31] proposed a similar mechanism during NO_x storage in which the bulk diffusion of a NO_x species through a densified barium nitrate phase limited the storage rate. However, ruling out either spillover mechanism requires a more detailed set of experiments and is under investigation.

The limitation of the supply of stored NO_x from the barium phase to Pt allows for a larger net production of NH_3 at lower temperatures because the H_2 front will propagate through the monolith faster at lower temperatures (breakthrough occurs with larger amounts of stored NO_x on the catalyst). Therefore the remaining stored NO_x is predominantly converted to NH_3 due to a Pt covered surface by H adatoms along the monolith.

Under H_2 feed rate limited conditions the route to N_2 is mainly dependent on the rate of H_2 and NO_x forming N_2 (path 2) and NH_3 (path 1) since all of the NH_3 is consumed, forming N_2 until breakthrough of H_2. Once H_2 breaks through the NH_3 formed will presumably exit the reactor without reacting due to the high concentrations of H_2 along the monolith. NH_3 formed after H_2 breakthrough may adsorb on the Pt and form NHx species, but due to high concentrations of H_2 and Pt-H the reverse reaction may also occur. A more detailed analysis of the route to N_2, direct or indirect is currently under investigation.

5. Conclusions

An in-depth study was performed on the reaction pathways during the regeneration of a $Pt/BaO/Al_2O_3$ monolith with H_2 as the reductant. The formation of N_2 can occur through four different reaction routes. The two primary routes are the reaction of H_2 with stored NO_x and the sequential route of stored NO_x reacting with H_2 forming NH_3 and then NH_3 reducing with stored NO_x downstream. The experiments show the occurrence of both routes. The sequential route is less favorable at lower temperatures (<230 °C) by comparing NH_3 and H_2 as reductants. Above 230 °C the reactivity of NH_3 and H_2 with stored NO_x are comparable.

The experiments reveal that the reduction process is initially feed rate limited by H_2. The rate limiting step switches from a feed rate limited state to one in which the supply of NO_x from the storage phase to Pt is limiting. This was observed by the breakthrough of H_2 and NH_3 prior to 100% conversion of the NO_x stored in the previous lean step. Conditions favorable for the supply of stored NO_x to be the rate limiting step was observed below 225 °C. H_2 and NH_3 breakthrough occurred at approximately 52% and 60% NO_x conversion at 180 and 225 °C, respectively. Above 275 °C, H_2 and NH_3 breakthrough occurred at nearly complete NO_x conversion.

The highest NO_x conversion obtained in our experiments was around 90%. As shown by the modeling studies of Sharma et al. [32], the NO_x conversion could be increased further either by increasing the length of the monolith piece (for fixed lean and rich phase times) or reducing the total cycle time (for a fixed length). The modeling studies by Sharma et al. [32] using propylene as reductant further showed that the NO_x conversion can approach 100% when less than 50% of the storage capacity (i.e. only the front part of the monolith) is used for storage during the lean phase so that the NO_x puff generated during the initial phase of the rich pulse does not escape but is readsorbed at the back half of the of the monolith and reduced subsequently. Since the commercial NO_x traps are 40–100 cm long, the spatiotemporal dynamics of the adsorption and temperature fronts play an important role in determining the optimal operating strategies. These and other aspects of the NO_x traps will be considered in a subsequent manuscript focused on the modeling studies.

Acknowledgements

The work reported was supported by the U.S. DOE National Energy Technology Laboratory (DE-FC26-05NT42630). We also acknowledge BASF Catalysts LLC for providing the catalysts used in this study.

References

[1] K.S. Kabin, P. Khanna, R.L. Muncrief, V. Medhekar, M.P. Harold, Catalysis Today 114 (1) (2006) 72–85.
[2] A. Scotti, I. Nova, E. Tronconi, L. Castoldi, L. Lietti, P. Forzatti, Industrial & Engineering Chemistry Research 43 (16) (2004) 4522–4534.
[3] L. Olsson, H. Persson, E. Fridell, M. Skoglundh, B. Andersson, Journal of Physical Chemistry B 105 (29) (2001) 6895–6906.
[4] E. Fridell, H. Persson, L. Olsson, B. Westerberg, A. Amberntsson, M. Skoglundh, Topics in Catalysis 16/17 (1–4) (2001) 133–137.
[5] W. Epling, L. Campbell, A. Yezerets, N. Currier, J. Parks, Catalysis Reviews 46 (2) (2004) 163–245.
[6] H. Abdulhamid, E. Fridell, M. Skoglundh, Topics in Catalysis 30/31 (1–4) (2004) 161–168.
[7] Z. Liu, J.A. Anderson, Journal of Catalysis 224 (1) (2004) 18–27.
[8] S. Poulston, R.R. Rajaram, Catalysis Today 81 (2003) 603–610.
[9] J. Theis, H.-W. Jen, R. McCabe, M. Sharma, V. Balakotaiah, M.P. Harold, Society of Automotive Engineers [Special Publication] SP, 2006, SP-2025 Advanced Catalysts and Substrates, 2006, pp. 69–82.
[10] R.L. Muncrief, K.S. Kabin, M.P. Harold, AIChE Journal 50 (10) (2004) 2526–2540.
[11] I. Nova, L. Lietti, L. Castoldi, E. Tronconi, P. Forzatti, Journal of Catalysis 239 (1) (2006) 244–254.
[12] I. Nova, L. Castoldi, L. Lietti, E. Tronconi, P. Forzatti, Society of Automotive Engineers [Special Publication] SP, SP-2022 (Diesel Exhaust), 2006, pp. 397–406.
[13] N.W. Cant, I.O.Y. Liu, M.J. Patterson, Journal of Catalysis 243 (2) (2006) 309–317.
[14] D. James, E. Fourre, M. Ishii, M. Bowker, Applied Catalysis B: Environmental 45 (2) (2003) 147–159.

[15] L. Olsson, H. Persson, E. Fridell, M. Skoglundh, B. Andersson, Journal of Physical Chemistry B 105 (2001) 6895–6906.
[16] J.A. Anderson, B. Bachiller-Baeza, M. Fernandez-Garcia, Physical Chemistry Chemical Physics 5 (2003) 4418–4427.
[17] G. Zhou, T. Luo, R.J. Gorte, Applied Catalysis, B: Environmental 64 (1/2) (2006) 88–95.
[18] V. Medhekar, V. Balakotaiah, M.P. Harold, Catalysis Today 121 (3/4) (2007) 226–236.
[19] J.-S. Choi, W.P. Partridge, W.S. Epling, N.W. Currier, T.M. Yonushonis, Catalysis Today 114 (1) (2006) 102–111.
[20] A. Lindholm, N.W. Currier, E. Fridell, A. Yezerets, L. Olsson, Applied Catalysis, B: Environmental 75 (1/2) (2007) 78–87.
[21] L. Lietti, P. Forzatti, I. Nova, E. Tronconi, Journal of Catalysis 204 (2001) 175–191.
[22] C.M.L. Scholz, V.R. Gangwal, M.H.J.M. de Croon, J.C. Schouten, Applied Catalysis, B: Environmental 71 (3/4) (2007) 143–150.
[23] H. Hu, DEER Conference, Detroit, USA, 2006.
[24] T. Morita, N. Suzuki, N. Satoh, K. Wada, H. Ohno, SAE (2007) 1–7.
[25] H.S. Gandhi, J.V. Cavataio, R.H. Hammerle, Y. Cheng, Catalyst system for the reduction of NO_x and NH3 emissions, US 7,332,135 (2002).
[26] J.A. Pihl, J.E. Parks II, C.S. Daw, T.W. Root, SAE Tech. Paper 2006-01-3441, 2006.
[27] L. Cumaranatunge, S.S. Mulla, A. Yezerets, N.W. Currier, W.N. Delgass, F.H. Ribeiro, Journal of Catalysis 246 (1) (2007) 29–34.
[28] J. Xu, R. Clayton, V. Balakotaiah, M.P. Harold, Applied Catalysis, B: Environmental 77 (3/4) (2008) 395–408.
[29] R. Clayton, M.P. Harold, V. Balakotaiah, Applied Catalysis, B: Environmental 81 (2008) 161–181.
[30] R.D. Clayton, M.P. Harold, V. Balakotaiah, AIChE, submitted (2008).
[31] U. Tuttlies, V. Schmeisser, G. Eigenberger, Chemical Engineering Science 59 (22/23) (2004) 4731–4738.
[32] M. Sharma, M.P. Harold, V. Balakotaiah, Industrial and Eng. Chem. Res. 44 (2004) 6264–6277.